

# Constraint on the velocity dependent dark matter annihilation cross section from gamma-ray and kinematic observations of dwarf galaxies

Yi Zhao<sup>1,2</sup>, Xiao-Jun Bi<sup>3,4</sup>, Peng-Fei Yin<sup>3</sup>, and Xinmin Zhang<sup>1,2,4</sup>

<sup>1</sup> *Theoretical Physics Center for Science Facilities,  
Chinese Academy of Sciences, Beijing 100049, China*

<sup>2</sup> *Theoretical Physics Division,*

<sup>3</sup> *Key Laboratory of Particle Astrophysics,  
Institute of High Energy Physics,*

*Chinese Academy of Sciences, Beijing 100049, China*

<sup>4</sup> *School of Physical Sciences,*

*University of Chinese Academy of Sciences,  
Beijing 100049, China*

Searching for  $\gamma$  rays from dwarf spheroidal galaxies (dSphs) is a promising approach to detect dark matter (DM) due to the high DM densities and low baryon components in dSphs. The Fermi-LAT observations from dSphs have set stringent constraints on the velocity independent annihilation cross section. However, the constraints from dSphs may change in velocity dependent annihilation scenarios because of the different velocity dispersions in galaxies. In this work, we set constraints on the velocity dependent annihilation cross section from the combined Fermi-LAT observations of dSphs with the kinematic data. In order to calculate the  $\gamma$  ray flux from the dSph, the correlation between the DM density profile and velocity dispersion at each position should be taken into account. We study such correlation and the relevant uncertainty from kinematic observations by performing a Jeans analysis. Using the observational results of three faint dSphs, including Willman 1, Reticulum II, and Triangulum II, we set constraints on the p-wave annihilation cross section in the Galaxy.

## 1. INTRODUCTION

Astrophysical and cosmological observations suggest that the universe is composed of  $\sim 4.8\%$  baryons,  $\sim 25.8\%$  cold dark matter (DM), and  $\sim 69.3\%$  dark energy [1]. Although DM is the dominant matter component in the universe, the nature of DM remains a mystery, and is beyond the framework of the standard model (SM). Many candidates for the DM particle have been proposed by the theorists, among which a kind of popular candidates is called the weakly interacting massive particle (WIMP) [2–4]. The observed DM relic density can be naturally explained by the current abundance of WIMPs in the thermal freeze-out scenario [5].

WIMPs are expected to annihilate or decay to SM particles in the universe, and could directly or indirectly produce  $\gamma$  rays. These  $\gamma$  ray signatures should be mainly generated in the regions with high DM densities, and then can be captured by detectors. The space-borne instrument Fermi Large Area Telescope (Fermi-LAT) is such a detector, which is sensitive to the  $\gamma$  rays from range 20 MeV to above 300 GeV [6]. Numerous works have been performed to study the  $\gamma$  ray signatures from DM annihilations in different astrophysical systems, such as the galaxy clusters [7], galactic halo [8–14], and galactic DM substructures [15–17].

Among these objects, the dwarf spheroidal satellite galaxies (dSphs) of the Milky Way are promising targets to look for the  $\gamma$  ray signatures from DM annihilation, because of their close proximity, high DM densities, low diffuse Galactic  $\gamma$ -ray foregrounds, and lack of conventional astrophysical  $\gamma$ -ray sources [18, 19]. So far, no significant  $\gamma$  ray signature over background in directions

of the known dSphs has been confirmed by Fermi-LAT observations. Therefore, the constraints on DM annihilation cross section in dSphs have been studied in numerous works [20–37].

The traditional s-wave DM annihilation process is independent of the relative velocity of DM particles. Its thermally averaged annihilation cross section accounting for the observed DM relic density is usually quoted at a canonical value  $\langle\sigma v\rangle \sim 3 \times 10^{-26} \text{ cm}^3\text{s}^{-1}$ . Nevertheless, the s-wave annihilation cross section has been constrained by the Fermi-LAT  $\gamma$ -ray observations from dSphs, which indicates  $\langle\sigma v\rangle$  should be smaller than the canonical value at low DM masses ( $\sim \mathcal{O}(1) - \mathcal{O}(10)$  GeV) for the annihilation channels to  $\tau^+\tau^-$  or  $b\bar{b}$  [29]. Note that  $\langle\sigma v\rangle$  generally depends on the relative velocity of DM particles. For instance, it can be expanded as  $\langle\sigma v\rangle = a + b\langle v^2\rangle + \mathcal{O}(v^4)$  in many models. If the p-wave annihilation is not negligible,  $\langle\sigma v\rangle$  is not a constant and would be suppressed at low DM velocities. In this case, due to the small DM velocity dispersions ( $\sim \mathcal{O}(1) - \mathcal{O}(10) \text{ km s}^{-1}$ ) in dSphs [38],  $\langle\sigma v\rangle$  in dSphs is smaller than those in the local Galactic halo and the early universe. Therefore, the constraints on the local Galactic  $\langle\sigma v\rangle$  derived from dSph  $\gamma$ -ray observations for velocity dependent annihilation scenarios may be weaker than those for the velocity independent annihilation scenario.

In this work, we study the constraint on the velocity dependent annihilation cross section from the Fermi-LAT dSph observations, taking into account the kinematic data. Some previous studies on the similar topic can be found in Ref. [33–37, 39, 40]. Note that in velocity dependent annihilation scenarios, the  $\gamma$ -ray flux from

a halo depend the DM number density and velocity dispersion in each position. Therefore, we should consider such correlation in the analysis rather than simply using a common velocity independent J factor. In order to take into account this effect and the related uncertainties from astrophysical observations, we use the package CLUMPY [41] to perform a Jeans analysis for the kinematic data of dSphs. By using these results, then we set constraints on the local  $\langle\sigma v\rangle$  in the Galaxy derived from dSph  $\gamma$ -ray observations. Although we only take p-wave annihilation as a benchmark scenario in the analysis, the application to other velocity dependent annihilation scenarios is straightforward.

This paper is organized as follows. In sec. 2, the statistical DM density distributions for dSphs are derived by a Jeans analysis. In sec. 3, we calculate the velocity dependent DM annihilation cross sections with the derived DM density files and velocity dispersions. Then we calculate the  $\gamma$ -ray flux from dSphs for p-wave annihilation, and consider the related uncertainties. By using the Fermi-LAT results, the constraints on the local Galactic  $\langle\sigma v\rangle$  are set. Section 4 is our conclusion.

## 2. ANALYSIS FOR DM DENSITY FILES OF DSPHS

### 2.1. Jeans analysis

We perform a Jeans analysis to obtain DM density profiles of dSphs. The motion of a collection of stars in a gravitational field can be described by Jeans equation, which is acquired from the collisionless Boltzmann equation. In the case of spherical symmetry, steady-state, and negligible rotational support, the second order Jeans equation is [42, 43]

$$\frac{1}{\nu(r)} \frac{d}{dr} [\nu(r)\sigma_r^2] + 2\frac{\beta_{ani}(r)\sigma_r^2}{r} = -\frac{GM(r)}{r^2}, \quad (1)$$

where  $\nu(r)$  is the three-dimensional stellar number density (3D light profile),  $\sigma_r^2$  is the radial velocity dispersion of tracers,  $\beta_{ani}(r) = 1 - \sigma_\theta^2/\sigma_r^2$  denotes the stellar velocity anisotropy depending on the ratio of tangential and radial velocity dispersions, and  $G$  is the gravitational constant. The enclosed mass in Eq. 1 is

$$M(r) = 4\pi \int_0^r \rho_{DM}(s)s^2 ds, \quad (2)$$

where  $\rho_{DM}$  is the DM density profile. The DM mass density profile rather than the total mass density profile used here is because the contribution of the stellar component is negligible compared to the DM halo. The solution to the three-dimensional Jeans equation is

$$\nu(r)\sigma_r^2 = \frac{1}{A(r)} \int_r^\infty A(s)\nu(s) \frac{GM(s)}{s^2} ds, \quad (3)$$

where  $A(r) = A_{r_1} \exp[\int_{r_1}^r \frac{2}{t} \beta_{ani}(t) dt]$ . However, astrophysical observations only provide the two-dimensional projected stellar number density and velocity dispersion along the line-of-sight. Therefore, the two-dimensional solution to the Jeans equation can be expressed as

$$\sigma_p^2(R) = \frac{2}{I(R)} \int_0^\infty [1 - \beta_{ani}(r) \frac{R^2}{r^2}] \nu(r) \sigma_r^2 dr, \quad (4)$$

where  $\sigma_p(R)$  is the projected velocity dispersion related to the projected radius  $R$ ,  $I(R)$  is the projected light profile (surface brightness).

We use the Markov Chain Monte Carlo (MCMC) toolkit GreAT embedded in the CLUMPY package [41] to solve the spherical Jeans equation. In Eq. 4, the surface brightness  $I(R)$  is fitted separately with a given parametric function. The parametric DM density profile  $\rho_{DM}$  and the velocity anisotropy  $\beta_{ani}$  should also be chosen. Then the Jeans analysis determine the parameters that can best reproduce the kinematic observations. When fitting to the kinematic data, the CLUMPY package provides two types of likelihood functions, namely the binned and unbinned likelihoods. If the kinematic data are in the form of binned velocity dispersion, we can use the binned likelihood function, while if the data are individual velocities along the line-of-sight, the unbinned likelihood function should be adopted. Compared with the binned likelihood analysis, the unbinned method does not introduce biases, and can reduce the statistical uncertainties, especially for the ultrafaint dSphs. In this work, we adopt the unbinned likelihood analysis to fit the kinematic data. The form of unbinned likelihood function is written as

$$\mathcal{L}_{unbin} = \prod_{i=1}^{N_{stars}} \left( \frac{\exp[-\frac{1}{2}(\frac{v_i - \bar{v}}{\sigma_p^2(R_i) + \Delta_{v_i}^2})]}{\sqrt{2\pi[\sigma_p^2(R_i) + \Delta_{v_i}^2]}} \right)^{P_i}, \quad (5)$$

where  $\sigma_p(R_i)$  is the projected velocity dispersion from Eq. 4,  $v_i$  is the velocity of the  $i$ -th star,  $\Delta_{v_i}$  is the uncertainty of velocity measurement, and  $P_i$  is the probability of membership for each star. The line-of-sight velocity is supposed as a Gaussian distribution, and  $\bar{v}$  is the mean velocity of the distribution.

### 2.2. Profile selection

We select three dSphs, namely Willman 1 (SDSS J1049+5103), Reticulum II (DES J0335.6-5403) and Triangulum II, in our analysis. These old and metal-poor stellar sources have almost the largest J-factors among known dSphs.

The stellar surface brightness is usually described by the Plummer profile [44], exponential profile [45], King profile [46], Sersic profile [47], or Zhao-Hernquist profile [48, 49]. We adopt the Plummer profile to fit the bright-

ness of these dSphs, which reads

$$I(R) = \frac{L}{\pi r_h^2} \frac{1}{(1 + \frac{R^2}{r_h^2})^2}, \quad (6)$$

where  $L$  is the total luminosity, and  $r_h$  is the projected half-light radius.

Willman 1 is a low-luminosity Milky Way satellite, which is located at  $(l, b) = (158.58^\circ, 56.78^\circ)$ . This source is an old, metal-poor stellar system at a distance of  $\sim 38$  kpc, with a half-light radius  $r_h \sim 21$  pc and an absolute magnitude  $M_V \sim -2.5$  [50–53]. The stellar density of Willman 1 with  $1\sigma$  uncertainties and background subtraction [52] is shown as Fig. 1, which is obtained from the Wide Field Camera (WFC) mounted on the Isaac Newton Telescope (INT). We fix the half-light radius of 0.021 kpc and fit the stellar density with the Plummer model, shown as the dashed line in this figure.

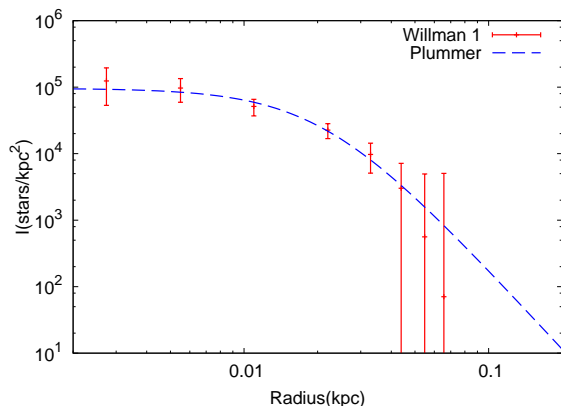


FIG. 1. The stellar density of Willman 1 with background subtracted. The blue dashed line represents the best fit given by the Plummer model.

Reticulum II was discovered from the recent optical imaging data collected during the first year of the Dark Energy Survey (DES). It is  $\sim 30$  kpc away and is located at  $(l, b) = (266.30^\circ, -49.74^\circ)$  with a half-light radius  $r_h \sim 32$  pc and an absolute magnitude  $M_V \sim -2.7$  [54–56]. The stellar density of Reticulum II [55] and fitting result are shown in Fig. 2. In the fit, we take a fixed half-light radius of 0.032 kpc. This value is taken into account the ellipticity of the object [55]. If the half-light radius is treated as a free parameter, the model provide a very good fit with  $r_h = 0.043$  kpc.

Triangulum II was discovered from the Panoramic Survey Telescope And Rapid Response System 3 $\pi$  imaging data. It is located at  $(l, b) = (140.90^\circ, -23.82^\circ)$ , with a heliocentric distance of  $\sim 30$  kpc, a half-light radius  $r_h \sim 34$  pc, and an absolute magnitude  $M_V \sim -1.8$  [57–59]. The stellar density of Triangulum II [57] is depicted in Fig. 3. We also adopt the Plummer model plus background to fit the data with a fixed half-light radius of 0.034 kpc.

A parametric DM density profile is required in the

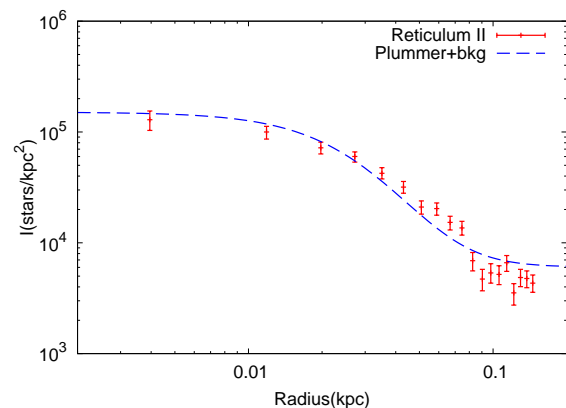


FIG. 2. The stellar density of Reticulum II. The blue dashed line represents the sum of the Plummer model result and background.

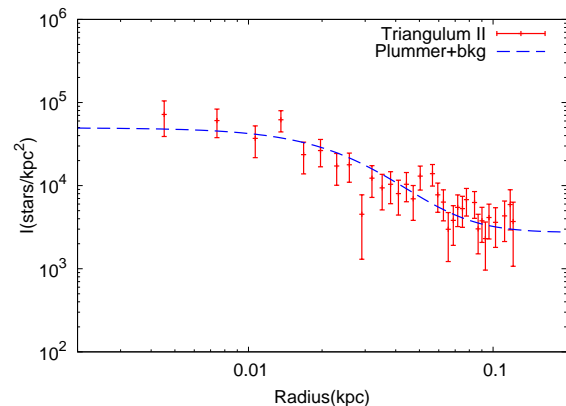


FIG. 3. The stellar density of Triangulum II. The blue dashed line represents the sum of the Plummer model result and background.

analysis. We use the Einasto [60] profile in this study, which is written as

$$\rho_{DM}(r) = \rho_{-2} \exp \left\{ -\frac{2}{\alpha} \left[ \left( \frac{r}{r_{-2}} \right)^\alpha - 1 \right] \right\}, \quad (7)$$

where  $\rho_{-2}$  is the normalization,  $r_{-2}$  is the scale radius corresponding to the profile slope at  $d \ln \rho / d \ln r = -2$ , and  $\alpha$  is the logarithmic slope. These three parameters are taken to be free parameters, and should be finally acquired by the fit.

Another more flexible form of the commonly used profile is the NFW [61] profile, which is also called the Zhao-Hernquist [48, 49] profile. This kind of profiles can be written as  $\rho_{DM}(r) = \frac{\rho_s}{(r/r_s)^\gamma [1 + (r/r_s)^\alpha]^{(\beta-\gamma)/\alpha}}$ , which relaxes the the transition slope  $\alpha$ , the outer slope  $\beta$  and the inner slope  $\gamma$ . Compared with the Einasto profile, this Zhao-Hernquist profile has more free parameters, and cause a slow MCMC running in the numerical analysis. Since the choice of these two kinds of profiles would not significantly affect the final results [62], we only con-

sider the Einasto profile in our study.

In the Jeans analysis, the stellar velocity anisotropy profile cannot be directly derived from measured stellar velocities, and therefore should be modeled or treated as a unknown factor. In this work we use a constant anisotropy model written as  $\beta_{ani}^{Const}(r) = \beta_0$ , of which the value is freely set in the MCMC algorithm. Another two different models can also be adopted in the analysis by the CLUMPY package. One is a simple anisotropy model proposed as  $\beta_{ani}^{Osipkov}(r) = r^2/(r^2 + r_a^2)$  in Ref. [63, 64], with a single parameter of scale radius  $r_a$ . Another model proposed by Baes & van Hese [65] is a more flexible one written as  $\beta_{ani}^{Baes}(r) = \frac{\beta_0 + \beta_\infty (r/r_a)^\eta}{1 + (r/r_a)^\eta}$ , where  $\beta_0$  and  $\beta_\infty$  are the anisotropies at the center and large radius respectively,  $\eta$  is the sharpness of the transition.  $\beta_{ani}^{Osipkov}(r)$  is a specific form of  $\beta_{ani}^{Baes}(r)$ , with the parameters  $\beta_0 = 0$ ,  $\beta_\infty = 1$ , and  $\eta = 2$ . For the classical dSphs, the Baes model is recommended to used in the fit, in order to take use of large stellar kinematic samples. However, this is not the case for the ultrafaint dSphs. Since the available stellar kinematic samples are few, it is difficult to clearly determine the anisotropy model for the ultrafaint dSphs considered in our study. Therefore, we take constant anisotropy model for simplicity.

In order to have a large statistics, we set 10 chains with  $10^5$  points per chain in the MCMC analysis. The priors of the DM density profile and the stellar velocity anisotropy models for three dSphs are listed in Tab. I. The validity of these priors has been discussed in Ref. [62].

TABLE I. Priors of the DM density profile (Einasto) and velocity anisotropy model (Constant) for three dSphs set in the MCMC analysis.

Parameter	Unit	Prior range
$\log_{10}(\rho_s)$	$(M_\odot/kpc^3)$	[5, 13]
$\log_{10}(r_s)$	$(kpc)$	[-1.6, 2]
$\alpha$	-	[0.12, 1]
$\beta_{ani}$	-	[-9, 1]

### 2.3. Kinematic data

We use the above approach to fit the observed kinematic data of each dSph. The kinematic data are in the form of coordinates and line-of-sight velocities with errors for individual stars. The member stars of the dSph are often contaminated by the Milky Way foreground stars. The membership probability  $P_i$  in Eq. 5 is such a weight parameter describing whether the  $i$ -th star belongs to the dSph. Some methods have been introduced to obtain the membership probability [66–69]. For the classical dSphs with large numbers of member stars, the membership probability of each star should be calculated one by one.

While for the ultrafaint dSphs, whose member stars are few, a binary classification ( $P_i = 0$  or  $P_i = 1$ ) for each star based on the velocity and line-strength criteria [70] is enough. The data of member stars in Willman 1, Reticulum II and Triangulum II are taken from Ref. [53], [56], and [58] respectively.

### 2.4. DM density profile and J factor

As mentioned above, we take the Einasto profile with three free parameters to model the DM density in the Jeans analysis. According to the posterior probability from the fit to dSph kinematic data, a set of density profiles for each dSph are given by the CLUMPY through the MCMC algorithm. We find that the number of derived profiles for Willman 1 is the smallest among the three dSphs. This is because that the kinematic samples of Willman 1 are larger than the other two, which result in a more efficient convergence in the fit.

A useful variable describing the dependence of the DM density distribution on the total annihilation rate is the so-called J factor. This factor is defined as the integration of the squared DM density along the line-of-sight over the solid angle

$$J = \int_{\Delta\Omega} \int_{l.o.s.} \rho^2(r) dl d\Omega. \quad (8)$$

The solid angle  $\Delta\Omega$  can be expressed as  $\Delta\Omega = 2\pi(1 - \cos\theta)$ , where  $\theta$  is the integral angle. Then we calculate the J factor for each density profile derived from the MCMC fit, and show their distributions in Fig. 4-6. In principle, the median value and variance of the J factor can be obtained from these results.

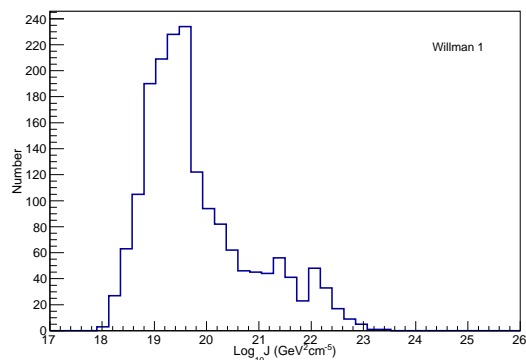


FIG. 4. The statistical distribution of J factors with integral angle  $0.5^\circ$  for Willman 1.

We display the J factors of each dSph with different integral angles for three dSphs in Fig. 7-9. In these figures, the red solid lines represent the median values of the J factor; the red dotted lines represent the 68% confidence intervals (CIs). In Ref. [71, 72], the J factors of Willman 1 and Reticulum II have been performed

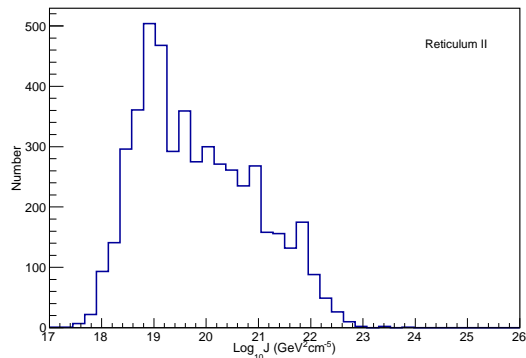


FIG. 5. The statistical distribution of  $J$  factors with integral angle  $0.5^\circ$  for Reticulum II.

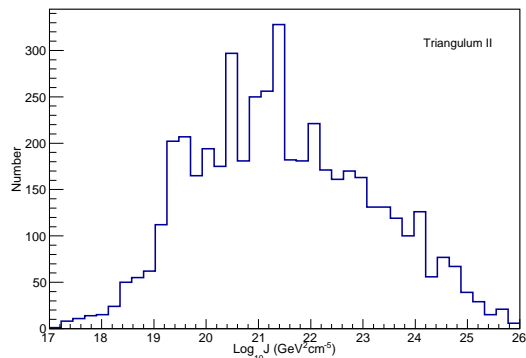


FIG. 6. The statistical distribution of  $J$  factors with integral angle  $0.5^\circ$  for Triangulum II.

with different light profiles and velocity anisotropy models. We also show their median values of the  $J$  factor as the blue dashed lines in Fig. 7 and 8 for comparison. We find that our results are consistent with those previous results. For instance, Ref. [71, 72] obtained  $\log_{10} J = 19.5^{+1.2}_{-0.6}$  and  $\log_{10} J = 19.6^{+1.0}_{-0.7}$  for Willman 1 and Reticulum II with an integral angle of  $0.5^\circ$  respectively, while we get these two values as  $\log_{10} J = 19.5^{+1.5}_{-0.6}$  and  $\log_{10} J = 19.6^{+1.4}_{-0.9}$ . The small difference between the  $1\sigma$  deviations may result from the different adopted light profiles and velocity anisotropy models.

For Triangulum II with an integration angle of  $0.5^\circ$ , we obtain  $\log_{10} J = 21.2^{+2.0}_{-1.6}$ , while the authors of Ref. [73] used the similar approach and reported a  $\log_{10} J = 20.9^{+1.4}_{-1.2}$ . The large uncertainty is mostly resulted from the few samples of member stars. Using the same package, the authors of Ref. [74] took the NFW DM profile, exponential light profile and constant velocity anisotropy model, and obtained a  $\log_{10} J = 21.03^{+0.83}_{-0.57}$ . The smaller variance compared with ours may be resulted from another set of kinematic data considered in their analysis, showing distinct stellar behaviors in the inner and outer regions of Triangulum II.

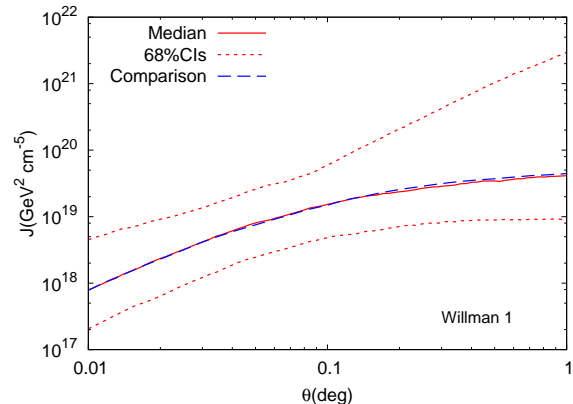


FIG. 7.  $J$  factor of Willman 1 as a function of integral angle. Red solid line and red dotted lines represent the median value and 68% CI respectively. The blue dashed line representing the result from Ref. [71] is also shown here for comparison.

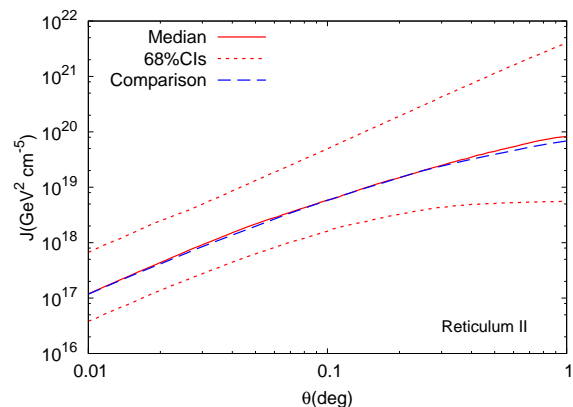


FIG. 8. The same as 7 but for Reticulum II. Also shown is the result from Ref. [72] for comparison.

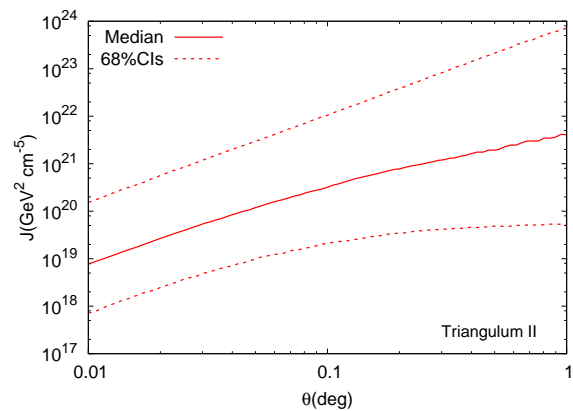


FIG. 9. The same as 7 but for Triangulum II.

### 3. LIMITS ON VELOCITY DEPENDENT ANNIHILATION CROSS SECTIONS

#### 3.1. DM annihilation cross section profile depending on relative velocities

In this section, we calculate the  $\gamma$ -ray fluxes from DM annihilations in dSphs and derive the related uncertainties. In general, the  $\gamma$ -ray flux is expressed as

$$\Phi = \frac{1}{8\pi m_{DM}^2} \int \frac{dN_\gamma}{dE_\gamma} dE_\gamma \int_{\Delta\Omega} \int_{l.o.s.} \langle\sigma v\rangle \rho^2 dl d\Omega, \quad (9)$$

where  $m_{DM}$  is the mass of DM and  $\frac{dN_\gamma}{dE_\gamma}$  is the differential  $\gamma$ -ray spectrum from one DM pair annihilation. In this work, we only consider the contribution to  $\frac{dN_\gamma}{dE_\gamma}$  from single annihilation channel given by PPPC4DM [75, 76].

For velocity independent DM annihilation, Eq. 9 can be rewritten by

$$\Phi = \frac{\langle\sigma v\rangle \cdot J}{8\pi m_{DM}^2} \int_{E_{min}}^{E_{max}} \frac{dN_\gamma}{dE_\gamma} dE_\gamma, \quad (10)$$

where  $J$  factor defined in the previous section is independent of  $\langle\sigma v\rangle$ . However Eq. 10 is not valid for the velocity dependent DM annihilation scenarios. Because the DM velocity distribution is not uniform in a DM halo,  $\langle\sigma v\rangle$  depending on the DM relative velocity changes at different positions. This means that  $\langle\sigma v\rangle$  cannot be simply moved from the integration in Eq. 9.

In principle, we can assume a modeling of the velocity dependent DM annihilation cross section as

$$\sigma v_{rel} = bF(v_{rel}), \quad (11)$$

where the function  $F(v)$  should be determined by the detailed model. Then  $\langle\sigma v\rangle$  at any position is given by

$$\langle\sigma v\rangle = b \cdot \int \int F(v_{rel}) f(v_1, \mathbf{r}) f(v_2, \mathbf{r}) dv_1^3 dv_2^3, \quad (12)$$

where  $f(v, \mathbf{r})$  is the DM velocity profile at position of  $\mathbf{r}$  and the relative velocity of two annihilating DM particles is given by  $v_{rel} = |\mathbf{v}_1 - \mathbf{v}_2|$ .

In this work, we assume the DM velocity distribution is a standard isotropic Maxwell-Boltzmann distribution. Although some studies have shown that deviations from the standard Maxwell-Boltzmann form are not negligible in large halos [77–80], we do not consider such effects for DM in dSphs. The DM velocity dispersion is determined by the Jeans equation for DM:

$$\frac{1}{\rho(r)} \frac{d}{dr} [\rho(r) \sigma_{D,r}^2] + 2 \frac{\beta_{D,ani}(r) \sigma_{D,r}^2}{r} = - \frac{GM(r)}{r^2}, \quad (13)$$

where  $\sigma_{D,r}^2$  and  $\beta_{D,ani}(r)$  are the radial velocity dispersion and anisotropy profile of DM respectively. With given  $\beta_{D,ani}(r)$ ,  $\sigma_{D,r}^2$  can be derived from Eq. 3 by replacing  $\nu(r)$ ,  $\sigma_r$  and  $\beta_{ani}$  with  $\rho(r)$ ,  $\sigma_{D,r}$  and  $\beta_{D,ani}$  respectively. As there is no enough information for the DM

velocity dispersion in dSphs, we simply take a isotropic velocity dispersion with  $\beta_{D,ani} = 0$ .

Then  $\langle\sigma v\rangle$  in the nonrelativistic limit is given by

$$\begin{aligned} \langle\sigma v\rangle &= b \int \sqrt{\frac{2}{\pi}} \frac{1}{v_p^3} v_{rel}^2 e^{-\frac{v_{rel}^2}{2v_p^2}} F(v_{rel}) dv_{rel} \\ &\equiv b \cdot g(r), \end{aligned} \quad (14)$$

where  $v_p^2 \sim 2\sigma_{D,r}^2$ . This means that  $\langle\sigma v\rangle$  is also a function of  $r$ . We define a factor  $C$  to take into account the dependence of the  $\gamma$  ray flux on the density profile:

$$\begin{aligned} C &= \int_{\Delta\Omega} \int_{l.o.s.} \rho^2(r) g(r) dl d\Omega \\ &= \int_0^{\theta_{max}} \int_{\theta-d}^{r_{max}} \frac{4\pi r \sin\theta \rho^2(r)}{\sqrt{r^2 - (\theta \cdot d)^2}} g(r) dr d\theta, \end{aligned} \quad (15)$$

where  $\theta_{max}$  is the maximum integral angle,  $d$  is the heliocentric distance of the dSph, and  $r_{max}$  is the maximum radius of the dSph. Finally, we can get the formula of  $\gamma$  ray flux for velocity dependent annihilation scenarios, which is similar to Eq. 10:

$$\Phi = \frac{b \cdot C}{8\pi m_{DM}^2} \int_{E_{min}}^{E_{max}} \frac{dN_\gamma}{dE_\gamma} dE_\gamma. \quad (16)$$

In a general WIMP scenario, the DM annihilation cross section is expanded as  $\sigma v_{rel} = a + b v_{rel}^2 + \mathcal{O}(v_{rel}^{2n})|_{n>1}$  in the nonrelativistic limit. In the following analysis, we take the pure p-wave annihilation scenario as a typical example with

$$\sigma v_{rel} = b v_{rel}^2. \quad (17)$$

According to the density profiles derived in the previous section, we can get the corresponding distributions of  $C$  factors for dSphs. We show such distributions for three selected dSphs in Fig. 10–12 and perform a gaussian fit. The mean values and variances of  $\log_{10} C$  are obtained as  $31.5 \pm 3.9$ ,  $32.5 \pm 3.4$  and  $34.7 \pm 4.5$  for Willman 1, Reticulum II, and Triangulum II, respectively.

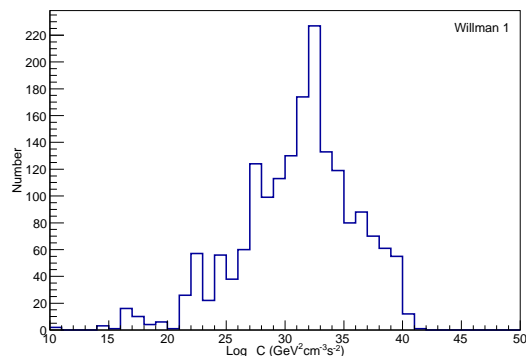


FIG. 10. Distribution of the  $C$  factor for Willman 1 within  $0.5^\circ$ .

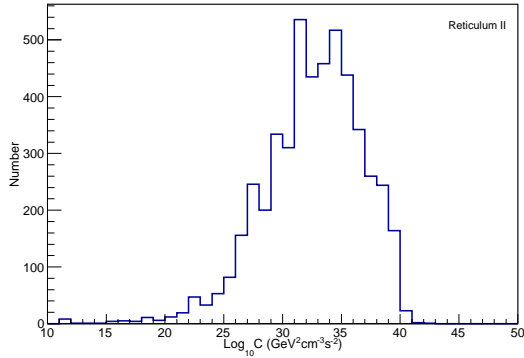


FIG. 11. Distribution of the C factor for Reticulum II within  $0.5^\circ$ .

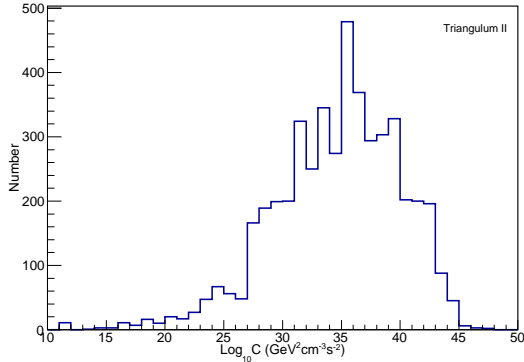


FIG. 12. Distribution of the C factor for Triangulum II within  $0.5^\circ$ .

### 3.2. limits on local DM annihilation cross sections

A maximum likelihood method has been developed for the Fermi-LAT  $\gamma$ -ray source analysis according to the limited photon statistics and the dependence of instrumental performance on the incident photon angle and energy. The Fermi-LAT collaboration has searched for  $\gamma$ -ray emissions from dozens of dSphs using Pass 8 data [22], including the three sources considered in this work. In that analysis, the data set consists of six-year results in the energy range from 500 MeV to 500 GeV, and is divided into 24 logarithmical energy bins. The “energy-flux-likelihood” information in the energy bin for each dSph has been provided<sup>1</sup>, and can be used for a grid scan in the likelihood analysis. According to Eq. 16 with a parameter set of  $m_{DM}$ ,  $b$  and  $C$ , the combined likelihood in all energy bins for the  $j$ -th dSph is estimated

as

$$\mathcal{L}_j = \prod_i \mathcal{L}_i(\Phi_i|D) \times \frac{e^{-[\log_{10}(C_j) - \log_{10}(C_{med,j})]^2 / 2\sigma_j^2}}{\ln(10)C_{mid,j}\sqrt{2\pi}\sigma_j}, \quad (18)$$

where  $i$  denotes the  $i$ -th energy bin,  $\Phi_i$  represents the corresponding DM signature flux, and  $C_{med,j}$  and  $\sigma_j$  are the obtained median value and variance of the C factor respectively. With given  $b$  and  $m_{DM}$ ,  $C_j$  is varied to make  $\mathcal{L}_j$  reach a maximum. The combined likelihood of several dSphs is calculated by

$$\mathcal{L} = \prod_j \mathcal{L}_j. \quad (19)$$

Then we can get upper limits on  $b$  at 95% C.L. by requiring that the corresponding  $\log \mathcal{L}$  has decreased by  $2.71/2$  from its maximum.

We translate the constraints on  $b$  to those on the local DM annihilation cross section in the Milky Way with a typical velocity dispersion of  $\sim 270 \text{ km s}^{-1}$ . Such limits are useful for the comparison between results from different DM indirect detection experiments. The results for the  $b\bar{b}$  and  $\tau^+\tau^-$  annihilation channels are shown in Fig. 13. The red solid line represents the limits from three selected dSphs on local pure p-wave annihilation with  $\sigma v_{rel} \sim b v_{rel}^2$ . For comparison, we also show the limits on velocity independent s-wave annihilation represented by blue solid lines, adopting the J factors obtained in our analysis. We find that they are stricter than those on p-wave annihilation by about four orders of magnitude. For any detailed model with a given ratio of  $a/b$ , the constraints on the DM annihilation cross section can be obtained straightforwardly.

Finally, we briefly discuss the impact of the choice of dSph samples. Although the J factors of the selected three dSphs are almost the largest among the known dSphs, including more known dSphs in the analysis will improve the constraints. The limits on the velocity independent annihilation cross section from the 41 dSphs combined analysis given by Ref. [22] are shown in Fig. 13. For comparison, we also show the limits for the three dSphs selected in our analysis in Fig. 13 as the green dashed lines, adopting the same J factors used in Ref. [22]<sup>2</sup>. It can be seen that enlarging the samples of known dSphs would improve the limits by a factor of  $\mathcal{O}(1)$  to 10.

<sup>2</sup> The differences between the results represented by blue solid and green dashed lines are caused by the J factors derived from different analysis. In Ref. [22], the J factors of Willman 1  $\log_{10} J = 18.9 \pm 0.6$  and Triangulum II  $\log_{10} J = 19.1 \pm 0.6$  are derived by a scaling relation between the distances and spectroscopically determined J factors of known dSphs, while the J factor of Reticulum II  $\log_{10} J = 18.9 \pm 0.6$  is taken from Ref. [81]. These J factors are different from those obtained in our analysis.

<sup>1</sup> [http://www-glast.stanford.edu/pub\\_data/1203/](http://www-glast.stanford.edu/pub_data/1203/)

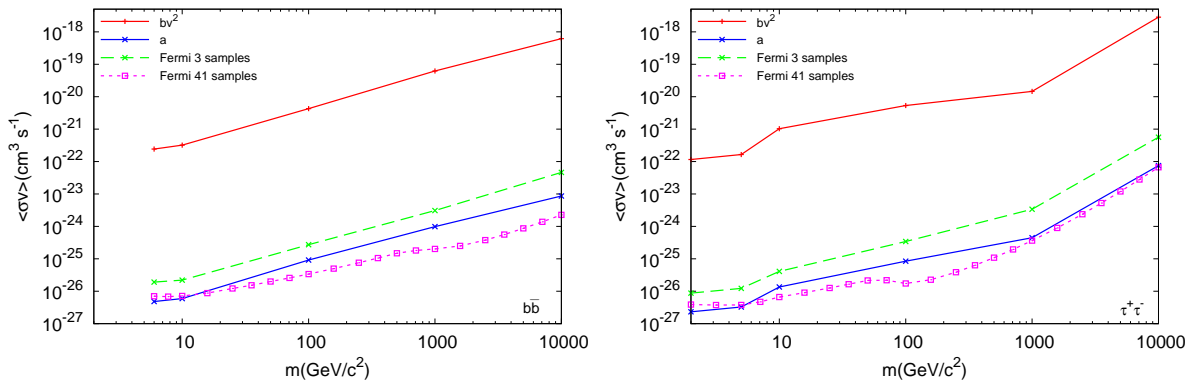


FIG. 13. Constraints on the DM annihilation cross section with a velocity dispersion of  $\sim 270 \text{ km s}^{-1}$  in the Galaxy at 95% C.L. for the  $b\bar{b}$  (left) and  $\tau^+\tau^-$  (right) channels. The red and blue solid lines represent the results for the pure p-wave annihilation and s-wave annihilation, respectively. These results are derived from a combined analysis of Fermi-LAT observations from Willman 1, Reticulum II and Triangulum II, with C factors and J factors obtained in this work. The green dashed lines are the same as blue solid lines but using the J factors as Ref. [22]. The pink dotted lines are given from a combined analysis for 41 dSphs in Ref. [22].

#### 4. CONCLUSIONS AND DISCUSSIONS

In this work, we study the constraints on the velocity dependent DM annihilation cross section from the Fermi-LAT  $\gamma$ -ray observations of dSphs. Since DM particles in different astrophysical systems have different velocity dispersions, their annihilation rates may significantly vary. Therefore, compared with ordinary analyses for the velocity independent annihilation scenario, the constraints on the DM annihilation cross section from dSphs observations would also change.

In order to calculate the  $\gamma$  ray flux from the dSph, the correlation of DM density profile and velocity dispersion at each position should be considered. In this work, we study such correlation and related uncertainty through Jeans analysis. We select three ultra-faint dSphs in the analysis, including Willman 1, Reticulum II, and Triangulum. These three sources have almost the largest J factors among the known dSphs. Through the Jeans analysis for kinematic data by using the package CLUMPY, a set of DM density profiles of these dSphs are given according to the posterior probability from the fit to kinematic data. We define a C factor to include the correlation between the DM density profile and velocity dispersion. The statistical distribution of C factor is given according to the DM density profiles derived from the Jeans analysis; the median value and variance can also be obtained.

We adopt the “energy-flux-likelihood” information of every energy bin for each dSph offered by the Fermi-LAT collaboration to set constraints on the  $\gamma$  ray flux. As an example, we set limits on the pure p-wave annihilation cross section in the Galaxy for the  $b\bar{b}$  and  $\tau^+\tau^-$  channels. By using the same procedure, the analyses for other velocity dependent annihilation scenarios and annihilation

channels are straightforward. Such results are useful to compare the results from different DM indirect detection experiments. Some velocity annihilation scenarios relax the general constraints from dSph observations, and can be used to explain some exotic results in observations. For instance, the DM explanation for the cosmic-ray  $e^\pm$  excess observed by AMS-02 has almost been excluded by the Fermi-LAT dSph observations in the velocity independent annihilation scenario, while this discrepancy can be relaxed in some velocity dependent annihilation scenarios.

In this work, we select three faint dSphs with large J factors in the Jeans analysis. Although the J factors of the three selected dSphs are almost the largest among known dSphs, there seems to exist some unclear uncertainties from the DM density density profile due to the few kinematic data of these ultra-faint dSphs. In principle, increasing the number of dSph samples would improve the final limits on the DM annihilation cross section. In the future, more dSphs may be discovered by observations. In order to search for the  $\gamma$  ray signature from velocity dependent DM annihilation, careful studies on DM density profile and velocity distribution are needed. More observational kinematic data and simulation results for dSphs will be necessary.

#### ACKNOWLEDGMENTS

We are grateful for the communications with Vincent Bonnard and David Maurin. This work is supported by the National Natural Science Foundation of China under Grants Nos. 11653001, 11375202, 11475191, 11475189, by the CAS pilot B program (No. XDB23020000), and by the National Key Program for Research and Development (No. 2016YFA0400200).

- 
- [1] Planck Collaboration, Adam, R., Ade, P. A. R., et al. 2016, *Astron. Astrophys.* , 594, A1
- [2] Jungman, G., Kamionkowski, M., & Griest, K. 1996, *Phys. Rept.* , 267, 195
- [3] Bergström, L. 2000, *Reports on Progress in Physics*, 63, 793
- [4] Bertone, G., Hooper, D., & Silk, J. 2005, *Phys. Rept.* , 405, 279
- [5] Steigman, G., Dasgupta, B., & Beacom, J. F. 2012, *Phys. Rev. D* , 86, 023506
- [6] Atwood, W. B., Abdo, A. A., Ackermann, M., et al. 2009, *Astrophys. J.* , 697, 1071
- [7] Ackermann, M., Ajello, M., Allafort, A., et al. 2010, *J. Cosmol. Astropart. Phys.* , 5, 025
- [8] Hooper, D., & Linden, T. 2011, *Phys. Rev. D* , 84, 123005
- [9] Ackermann, M., Ajello, M., Atwood, W. B., et al. 2012, *Astrophys. J.* , 761, 91
- [10] Abazajian, K. N., & Kaplinghat, M. 2012, *Phys. Rev. D* , 86, 083511
- [11] Abdo, A. A., Ackermann, M., Ajello, M., et al. 2010, *Physical Review Letters*, 104, 091302
- [12] Ackermann, M., Ajello, M., Albert, A., et al. 2012, *Phys. Rev. D* , 86, 022002
- [13] Weniger, C. 2012, *J. Cosmol. Astropart. Phys.* , 8, 007
- [14] Ackermann, M., Ajello, M., Albert, A., et al. 2013, *Phys. Rev. D* , 88, 082002
- [15] Zechlin, H.-S., Fernandes, M. V., Elsässer, D., & Horns, D. 2012, *Astron. Astrophys.* , 538, A93
- [16] Ackermann, M., Albert, A., Baldini, L., et al. 2012, *Astrophys. J.* , 747, 121
- [17] Zechlin, H.-S., & Horns, D. 2012, *J. Cosmol. Astropart. Phys.* , 11, 050
- [18] Mateo, M. L. 1998, *Annu. Rev. Astron. Astrophys.* , 36, 435
- [19] Grcevich, J., & Putman, M. E. 2009, *Astrophys. J.* , 696, 385
- [20] Abdo, A. A., Ackermann, M., Ajello, M., et al. 2010, *Astrophys. J.* , 712, 147
- [21] Ackermann, M., Ajello, M., Albert, A., et al. 2011, *Physical Review Letters*, 107, 241302
- [22] Albert, A., Anderson, B., Bechtol, K., et al. 2017, *Astrophys. J.* , 834, 110
- [23] Geringer-Sameth, A., & Koushiappas, S. M. 2011, *Physical Review Letters*, 107, 241303
- [24] Cholis, I., & Salucci, P. 2012, *Phys. Rev. D* , 86, 023528
- [25] Geringer-Sameth, A., & Koushiappas, S. M. 2012, *Phys. Rev. D* , 86, 021302
- [26] Mazziotta, M. N., Loparco, F., de Palma, F., & Giglietto, N. 2012, *Astroparticle Physics*, 37, 26
- [27] Baushev, A. N., Federici, S., & Pohl, M. 2012, *Phys. Rev. D* , 86, 063521
- [28] Huang, X., Yuan, Q., Yin, P.-F., Bi, X.-J., & Chen, X. 2012, *J. Cosmol. Astropart. Phys.* , 11, 048
- [29] Ackermann, M., Albert, A., Anderson, B., et al. 2014, *Phys. Rev. D* , 89, 042001
- [30] Fermi-LAT Collaboration 2015, arXiv:1503.02641
- [31] Sming Tsai, Y.-L., Yuan, Q., & Huang, X. 2013, *J. Cosmol. Astropart. Phys.* , 3, 018
- [32] Zhao, Y., Bi, X.-J., Yin, P.-F., & Zhang, X.-M. 2017, arXiv:1702.05266
- [33] Essig, R., Sehgal, N., Strigari, L. E., Geha, M., & Simon, J. D. 2010, *Phys. Rev. D* , 82, 123503
- [34] Zhao, Y., Bi, X.-J., Jia, H.-Y., Yin, P.-F., & Zhu, F.-R. 2016, *Phys. Rev. D* , 93, 083513
- [35] Choquette, J., Cline, J. M., & Cornell, J. M. 2016, *Phys. Rev. D* , 94, 015018
- [36] Boddy, K. K., Kumar, J., Strigari, L. E., & Wang, M.-Y. 2017, *Phys. Rev. D* , 95, 123008
- [37] Lu, B.-Q., Wu, Y.-L., Zhang, W.-H., & Zhou, Y.-F. 2017, arXiv:1711.00749
- [38] Walker, M. G., Mateo, M., Olszewski, E. W., et al. 2009, *Astrophys. J.* , 704, 1274
- [39] Campbell, S., Dutta, B., & Komatsu, E. 2010, *Phys. Rev. D* , 82, 095007
- [40] Campbell, S., & Dutta, B. 2011, *Phys. Rev. D* , 84, 075004
- [41] Bonnavard, V., Hütten, M., Nezri, E., et al. 2016, *Computer Physics Communications*, 200, 336
- [42] Binney, J., & Tremaine, S. 2008, *Galactic Dynamics: Second Edition*, by James Binney and Scott Tremaine. ISBN 978-0-691-13026-2 (HB). Published by Princeton University Press, Princeton, NJ USA, 2008.
- [43] Courteau, S., Cappellari, M., de Jong, R. S., et al. 2014, *Reviews of Modern Physics*, 86, 47
- [44] Plummer, H. C. 1911, *Mon. Not. Roy. Astron. Soc.* , 71, 460
- [45] Evans, N. W., An, J., & Walker, M. G. 2009, *Mon. Not. Roy. Astron. Soc.* , 393, L50
- [46] King, I. 1962, *Astron. J.* , 67, 471
- [47] Sersic, J. L. 1968, *Cordoba, Argentina: Observatorio Astronomico*, 1968
- [48] Zhao, H. 1996, *Mon. Not. Roy. Astron. Soc.* , 278, 488
- [49] Hernquist, L. 1990, *Astrophys. J.* , 356, 359
- [50] Willman, B., Blanton, M. R., West, A. A., et al. 2005, *Astron. J.* , 129, 2692
- [51] Willman, B., Masjedi, M., Hogg, D. W., et al. 2006, arXiv:astro-ph/0603486
- [52] Martin, N. F., Ibata, R. A., Chapman, S. C., Irwin, M., & Lewis, G. F. 2007, *Mon. Not. Roy. Astron. Soc.* , 380, 281
- [53] Willman, B., Geha, M., Strader, J., et al. 2011, *Astron. J.* , 142, 128
- [54] Bechtol, K., Drlica-Wagner, A., Balbinot, E., et al. 2015, *Astrophys. J.* , 807, 50
- [55] Koposov, S. E., Belokurov, V., Torrealba, G., & Evans, N. W. 2015, *Astrophys. J.* , 805, 130
- [56] Walker, M. G., Mateo, M., Olszewski, E. W., et al. 2015, *Astrophys. J.* , 808, 108
- [57] Laevens, B. P. M., Martin, N. F., Ibata, R. A., et al. 2015, *Astrophys. J. Lett.* , 802, L18
- [58] Kirby, E. N., Cohen, J. G., Simon, J. D., & Guhathakurta, P. 2015, *Astrophys. J. Lett.* , 814, L7
- [59] Martin, N. F., Ibata, R. A., Collins, M. L. M., et al. 2016, *Astrophys. J.* , 818, 40
- [60] Merritt, D., Graham, A. W., Moore, B., Diemand, J., & Terzić, B. 2006, *Astron. J.* , 132, 2685
- [61] Navarro, J. F., Frenk, C. S., & White, S. D. M. 1997, *Astrophys. J.* , 490, 493
- [62] Bonnavard, V., Combet, C., Maurin, D., & Walker, M. G. 2015, *Mon. Not. Roy. Astron. Soc.* , 446, 3002
- [63] Osipkov, L. P. 1979, *Pisma v Astronomicheskii Zhurnal*, 5, 77

- [64] Merritt, D. 1985, *Astron. J.* , 90, 1027
- [65] Baes, M., & van Hese, E. 2007, *Astron. Astrophys.* , 471, 419
- [66] Walker, M. G., Mateo, M., Olszewski, E. W., Sen, B., & Woodroffe, M. 2009, *Astron. J.* , 137, 3109
- [67] Martinez, G. D., Bullock, J. S., Kaplinghat, M., Strigari, L. E., & Trotta, R. 2009, *J. Cosmol. Astropart. Phys.* , 6, 014
- [68] Klimentowski, J., Lokas, E. L., Kazantzidis, S., et al. 2007, *Mon. Not. Roy. Astron. Soc.* , 378, 353
- [69] Wojtak, R., & Lokas, E. L. 2007, *Mon. Not. Roy. Astron. Soc.* , 377, 843
- [70] Simon, J. D., & Geha, M. 2007, *Astrophys. J.* , 670, 313
- [71] Bonnivard, V., Combet, C., Daniel, M., et al. 2015, *Mon. Not. Roy. Astron. Soc.* , 453, 849
- [72] Bonnivard, V., Combet, C., Maurin, D., et al. 2015, *Astrophys. J. Lett.* , 808, L36
- [73] Hütten, M., Combet, C., Maier, G., & Maurin, D. 2016, *J. Cosmol. Astropart. Phys.* , 9, 047
- [74] Genina, A., & Fairbairn, M. 2016, *Mon. Not. Roy. Astron. Soc.* , 463, 3630
- [75] Cirelli, M., Corcella, G., Hektor, A., et al. 2011, *J. Cosmol. Astropart. Phys.* , 3, 051
- [76] Ciafaloni, P., Comelli, D., Riotto, A., et al. 2011, *J. Cosmol. Astropart. Phys.* , 3, 019
- [77] Fairbairn, M., & Schwetz, T. 2009, *J. Cosmol. Astropart. Phys.* , 1, 037
- [78] Vogelsberger, M., Helmi, A., Springel, V., et al. 2009, *Mon. Not. Roy. Astron. Soc.* , 395, 797
- [79] Zemp, M., Diemand, J., Kuhlen, M., et al. 2009, *Mon. Not. Roy. Astron. Soc.* , 394, 641
- [80] Kuhlen, M., Weiner, N., Diemand, J., et al. 2010, *J. Cosmol. Astropart. Phys.* , 2, 030
- [81] Simon, J. D., Drlica-Wagner, A., Li, T. S., et al. 2015, *Astrophys. J.* , 808, 95